Fabrication and Characterization of Multifunctional Silicon Nitride Blow-Spun Nanofibers for Wound Healing Applications

Femi K Alakija and David Mills *

Posted Date: 6 June 2025

doi: 10.20944/preprints202506.0475.v1

Keywords: solution blow spinning; halloysite nanotube; magnesium oxide; silicon nitride; antimicrobial; wound healing

 doi:10.20944/preprints202506.0475.v1

Article

Fabrication and Characterization of Multifunctional Silicon Nitride Blow Spun Nanofibers for Wound Healing Applications

Femi Alakija[1] and David K. Mills[1,2,*]

[1] Molecular Science and Nanotechnology

[2] School of Biological Sciences, Louisiana Tech University, Ruston, LA 71272

* Correspondence: dkmills@latech.edu; Tel.: (318) 257-2640; Fax (318) 257-4574

Abstract: Wound healing is a critically essential but complex process requiring intense or prolonged medical intervention to achieve positive clinical outcomes. In addition, the increasing prevalence of chronic nonhealing wounds places a significant burden on a patient's quality of life and a sizeable financial strain on healthcare providers, especially as the treatment options are limited. This research aimed to fabricate multifunctional antimicrobial nanocomposite fibers with enhanced mechanical properties to facilitate wound healing and reduce microbial infection. We used a patented electrodeposition process to coat magnesium (MgO) on the halloysite (HNT) outer surface. Using the solution blow spinning technique, nanocomposite fibers were spun as a square (4 in X 4 in) onto sterile gauze. Material characterization was used to confirm the presence of MgO on the HNT outer surface. Antimicrobial activity was tested against *Escherichia coli* and *Staphylococcus aureus*. The effects of nanocomposite fiber on human fibroblast cell response were also evaluated. An in-vitro wound healing assay assessed the wound healing potential of the MgO/HNT composite fibers. SEM images showed the presence of Mg on the HNT surface, which Energy Dispersive Spectroscopy confirmed. Cytotoxicity tests showed that the composite fibers were not toxic to mammalian cells. Cell proliferation assays showed that Si3N4 enhanced proliferation. The nanocomposite fibers also promoted cell migration into an in vitro "mechanical wound" created by the scratch assay.

Keywords: solution blow spinning; halloysite nanotube; magnesium oxide; silicon nitride; antimicrobial; wound healing

1. Introduction

The largest organ in the body is the skin, which acts as a barrier against the entry of foreign pathogens, thermoregulation, and sensation [1]. Given the skin's numerous functions, one can only imagine the problems that might arise when the skin is injured or not functioning correctly. Injuries can damage a victim's psychological well-being and endanger the skin barrier's function as a defense mechanism. If wounds are not treated, they may turn fatal. Also, the pathogens are not eliminated during an injury. In that case, the tissue is further invaded, and it impedes wound healing depending on the degree of the injury and the immune system's strength. However, some bacteria need moisture and nutrients at the wound site to grow when they invade a wound. Therefore, the amount of nutrients that are available to the cells that are growing is limited. Invasion of bacteria at a wound site can make the wound chronic and more difficult to treat [2]. The largest organ in the body is the skin, which acts as a barrier against the entry of foreign pathogens, thermoregulation, and sensation [1]. Given the skin's numerous functions, one can only imagine the problems that might arise when the skin is injured or not functioning correctly. Injuries can damage a victim's psychological well-being and endanger the skin barrier's function as a defense mechanism. If wounds are not treated, they may turn fatal. Also, the pathogens are not eliminated during an injury. In that case, the tissue

 doi:10.20944/preprints202506.0475.v1

is further invaded, and it impedes wound healing depending on the degree of the injury and the immune system's strength. However, some bacteria need moisture and nutrients at the wound site to grow when they invade a wound. Therefore, the amount of nutrients that are available to the cells that are growing is limited. Invasion of bacteria at a wound site can make the wound chronic and more difficult to treat [2].

Nearly 6.5 million people in the U.S. experience chronic wounds each year, and that expense amounts to about $25 billion annually [2-4]. Therefore, an enormous amount of interest has been shown in wound dressings that contain antimicrobial agents to prevent bacterial invasion of the wound site. The bacteria and cells in wound healing compete at the wound site. However, if they adhere first, bacteria are more likely to take over the wound site.

There are several types of materials used in wound dressings. For example, Nonwoven textiles prepared from hyaluronan (HA) have low porosity, non-toxicity, and excellent mechanical strength [5]. Suitable wound dressing materials should have hemostatic [6,7] and anti-inflammatory properties [8,9], be non-toxic [10], be able to provide gas exchange [11], have fibroblast and keratinocyte proliferation, and easily remove without irritating. Unnecessary changes in wound dressings can be painful and lead to injury, thereby creating disturbances in the process. Therefore, several nanoparticles have been loaded into electrospun textiles for wound-healing applications [12]. For example, AgNPs are loaded into an electrospun textile with kaolinite to inhibit bacteria growth by opening the bacteria cell membrane [13].

Electrospinning is the fundamental technology for fabricating fiber materials [14]. However, in recent years, solution blow spinning (SBS) has started to gain the attention of researchers due to its advantages over electrospinning and other spinning techniques such as melt blown, centrifugal spinning, and magnetic-mechanical spinning [15,16]. SBS is an inexpensive, simple apparatus technique that involves using two fluids: a solvent to dissolve the polymer and a pressurized gas. SBS setup consists of a syringe pump, an airbrush, and a compressed gas [17]. SBS technology and large-scale fabrication can use different ranges of materials. In addition, SBS is helpful in the fabrication technique where a voltage-sensitive polymer is involved since it does not require voltage use [18].

Lou et al. (2013) demonstrated a way to fabricate micro/nanofibers by investigating four factors of SBS, which include injection rate, air pressure, solution concentration, and the nozzle diameter by fabricating polyethylene oxide (PEO) micro/nanofibers and concluded that these four factors affected the fabricated fiber diameter [19]. Some of the limitations of SBS include the uneven distribution of fibers leading to poor fiber morphology, the polymer concentration type, liquid intake, atmospheric and gas pressure, and the working distance [18]. The solvent evaporation rate is one of the advantages of SBS over other spinning techniques.

Magnesium oxide (MgO) has been shown to have excellent antibacterial properties against *E. coli* [20], *B. subtilis, and B. megaterium* [21] mycobacterium tuberculosis [22] by destroying their cell membrane, which will cause the release of the cell content and in turns cell death [23]. MgO is superior to other nanoparticles such as Ag, Cu, and TiO_2 because of its precursor availability, biocompatible, and excellent antibacterial properties [20]; this establishes their application in waste management, electronics, medical industry, as well as orthopedic for bone regeneration [20].

Silicon nitride (Si_3N_4) may be a potential therapeutic option for treating bone diseases and physiologically regulating the processes of bone development [24]. The biological relationship between living cells and Si_3N_4 was investigated, and their findings were built upon prior research [25] and indicated that Si_3N_4 has medicinal therapies for joint diseases [26]. Si_3N_4 is optimized to give a zwitterionic-like property showing improved osteoconductive and cell adhesion, making them applicable as bone substitutes and containing anti-fouling properties [27]. Due to Si_3N_4 properties, it was shown to have applications in drug delivery [28], orthopedics [29], and antimicrobial agents [30]. For example, Si_3N_4 was used to fabricate total hip arthroplasty bearing and compared with bearing fabricated with only Al_2O_3, which shows inferior fracture toughness and strength compared to reinforcing Si_3N_4 with Al_2O_3, which produces more improved properties [31].

 doi:10.20944/preprints202506.0475.v1

Halloysite nanotubes (HNTs) are a type of nanomaterial that is naturally available and abundant in clay particles [32]. Halloysite nanotubes are double-layered aluminosilicate nanoclay with a predominantly hollow tubular structure. It has a chemical formula of $Al_2Si_2O_5(OH)_{4n}H_2O$. HNTs have an external diameter of 50 – 80 nm, an inner lumen of 10 - 15 nm, and a length of 1 µm [33]. Each cylinder has concentric alternating layers of aluminum and silicate, giving the cylinder or tube positive and negatively charged layers. These alternating charges make halloysite nanoparticles suitable adsorbents for cations and anions. HNTs are abundantly and commercially available cheaply ($15/metric ton), attracting increased interest across engineering and science disciplines [34]. HNTs were reported to be non-toxic and biocomposite. Due to the weak intermolecular forces of HNT, they must undergo surface modification by reinforcing them with other materials to improve their properties. For instance, surface modification of HNT with bis(triethoxysilylpropyl)-tetrasulfide resulted in superior thermal stability and physical properties compared to the HNT without modification [35].

This study shows the potential of Si_3N_4 and magnesium-coated HNTs (MgO/HNTs) fibers and their bacteriostatic activity. Furthermore, the effect that the silicon nitride and MgO/HNT concentration and their combined ratio have on the antimicrobial properties of the blow-spun nanocomposite fibers were equally analyzed. In addition, the effect of these polymers on the cell in vitro for fibroblast cells was demonstrated.

Materials and Methods

Chemicals and Reagents

Magnesium oxide (CAS: 1309-48-4), halloysite nanoclay (LOT: 685445-500G, CAS: 1332-58-7), senescence cell histochemical staining kit (CAT: #CS0030-1KT), and gentamicin sulfate salt (LOT #049M4874V) were obtained from Sigma-Aldrich, St. Louis, MO. Dulbecco's modified eagle's medium (DMEM) (LOT: 2393824) and penicillin/streptomycin (REF: 15070-063) were obtained from Gibco Invitrogen, Grand Island, NY. Fetal bovine serum (FBS) (CAT: FBS002, LOT: N21H21) was obtained from Neuromics, Edima, MN. Cell counting kit-8 (CAT: #DJDB4000X) was from Vita Scientific, college park, MD. The Biotium viability/cytotoxicity assay kit (CAT: 30002-T, LOT: 210811) was from Biotium, Fremont, CA. Polylactic acid and Silicon nitride (CAS; 12033-89-5) were obtained from 3DTech, Grand Rapids, MI, and Chem Savers, Bluefield, VA, respectively. Acetone (CAS: 67641) was obtained from Emplura-Millipore Sigma, Burlington, MA. Phosphate buffer saline (PBS; REF: 25-508B; LOT: MS00LB) was from Genesee Scientific, San Diego, CA. Human dermal fibroblast cells (HDF, PCS-201-012, LOT #81201212), *Escherichia coli* (ATCC 25922), and *Staphylococcus aureus* (ATCC 6538) were obtained from ATCC, Manassas, VA. Cytoselect™ 24-well cell migration assay, 8 µm, Fluorometric format (CAT: #CBA-101) was obtained from Cell Biolabs, San Diego, CA.

Electrodeposition of Magnesium Oxide on HNTs (MgO/HNT)

A platinum-coated titanium mesh electrode electrodeposition consists of two electrodes that operate as a reversible cathode and anode. The electrodes were cleaned using silicon carbide abrasive sandpaper to remove pollution before being ultrasonically sonicated in pure water for 10 minutes. A DC source was linked to the two electrodes spaced two inches apart (20 V). 350 mg of HNT and 141.07 mg of MgO were blended and dispensed into a solution of 700 mL of water at 85°C in the electrolysis vessels. The solution was continually agitated using a magnetic stir bar to promote formation at the working electrode while reducing electrophoretic accumulation. After 5 minutes, the polarity was switched back for 30 minutes (6 cycles). About five minutes were given for the solution to settle before the supernatant was decanted and three times rinsed with deionized water. The solution was centrifuged for 5 minutes at 2000 rpm to eliminate NPs that had not yet reacted to the supernatant. the MgO/HNT were dried at 37 °C.

Fabrication of Antimicrobial Blow-Spun Nanocomposite Fibers

 doi:10.20944/preprints202506.0475.v1

Fabrication started with solvent selection based on FDA-approved materials, after which suitable solvents were used. Three compositions were tested in this study: Si_3N_4/PLA, MgO/HNT/PLA, and Si_3N_4MgO/HNT/PLA. The experiment was prepared in two concentrations (25% and 30%), as shown in Figure 1. For 25% Si_3N_4 MgO/HNT/PLA, 1 g of PLA was added to a blended mixture of 0.150 g of Si_3N_4 and 0.150 g of MgO/HNT in a reagent bottle. The solvent choice was Chloroform and acetone in a 50:50 proportion. Next, 20 mL of the solvent was added to the sample reagent bottle and placed at room temperature for 48 hours to dissolve. The fibers were blown onto a square (4 in X 4 in) sterile gauze using the solution blow spinning technique, after which the gauze was dried at room temperature overnight.

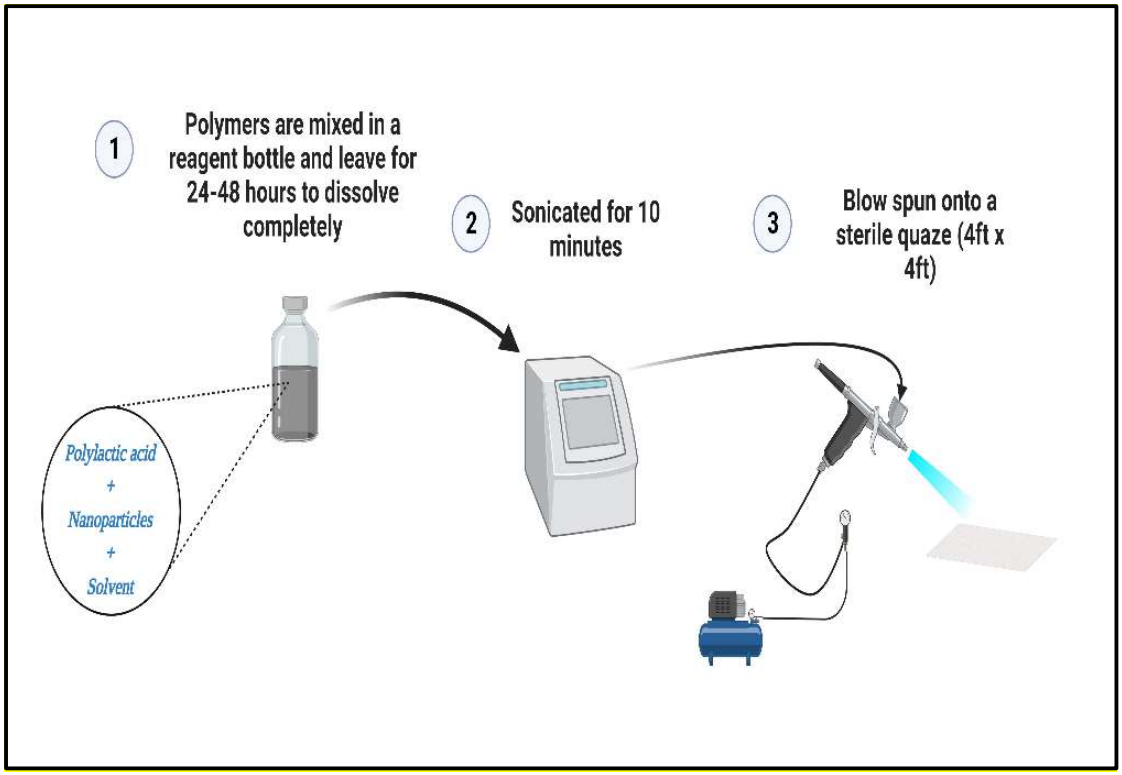

Figure 1. Schematic illustrating the fiber fabrication process. (Figure created through BioRender.com).

Materials Characterization

Scanning Electron Microscope (SEM) and Digital Microscopy

The surface morphologies of MgO/HNT were studied using a Hitachi S4800 Field Emission SEM, and the image that resulted was used to verify that the HNTs are coated with the MgO nanoparticles.

Energy Dispersive Spectroscopy (EDS)

MgO/HNT were subsequently examined to determine the elemental presence and the weight % of MgO on the HNTs with the aid of the EDAX dispersive X-ray analyzer attached to the SEM.

Evaluation of In Vitro Fibroblast Response

Cell Culture and Culture Medium

Cryopreserved cells were purchased from ATCC, thawed, and equilibrated in a water bath. The complete culture media contains an alpha modification of Eagle's medium (DMEM) containing 10% fetal bovine serum (FBS) and 1% penicillin/streptomycin antibiotic. The medium was filtered with vacuum filtration to remove large particles and contamination. Human dermal fibroblast (HDF) was

 doi:10.20944/preprints202506.0475.v1

thawed and cultured in the filtered DMEM complete media and then stored in a humidified incubator at 37°C and 5% CO_2 level. Cells were allowed to attain 90-95% confluency and passaged with 0.25% trypsin. Cell culture plates were purchased from Midscientific, St. Louis, MO. Sub-confluent cells were passaged with 2 mL 0.25% Trypsin, centrifuged at 3000 rcf for 3-5 minutes, and resuspended in 2 mL of media.

Sample Conditioning

After being sterilized by UV light, 163 mg–165 mg of blown-spun nanocomposite fibers was extracted by conditioning in 5 mL of DMEM complete media for 72 hours at 37°C. 5 mL of fresh DMEM complete medium was added to the diluted extraction and mixed.

Cell Proliferation Assay Test

Nexcelon Bioscience Auto T4 Cellometer cell counter was used for cell counting to get 1 X 10^5 cells/well. The conditioned nanocomposite fibers were inoculated with 100 µL/well cell suspension (1 X 10^5 cells/well) in a 96-well cell culture plate and incubated at 37°C until attaining confluence. After attaining confluence, the Cell counting kit-8 reagent (Vita scientific, Cat #DJDB4000X) was thawed, and 1/10 µL/well of total cells was added to the cell culture plate for "x" day and incubated at 37°C for 1-4 hours. BioTek Instruments, Inc., REF 800TS microplate reader was used to record the optical density (OD) at 450 nm. "x" was day 1, 3, 5, and *Cytotoxicity Testing*

Assessing the combined cytotoxicity of Si_3N_4, MgO, and HNT on biological cells is crucial. After being exposed to human dermal fibroblast cell culture (500 µL of cell/well), the conditioned nanocomposite blow-spun fibers were subjected to a live/dead experiment to determine the cell viability using the biotium viability/cytotoxicity assay kit (Cat: 30002-T, Lot:210811) in a 24- well plate to attain 90-95% confluency in a 37°C incubator. After attaining confluence, the Cells were washed with 300 µL PBS twice before staining with the biotium solution and then incubated at room temperature for 30-45 minutes. Cytotoxicity was assessed on day 1, 3, 5, and 7 while utilizing Image J for live and dead counting.

Scratch Assay

The scratch assay is a mechanical wounding assay used to analyze in vitro cell migration and measures three essential parameters: speed of migration, persistence, and polarity of migration. First, cells were counted and seeded in a 24-well, and after the cells had attained confluency, a scratch was introduced with a sterilized 200 µL pipette tip. After the wounding step, how the cell behaves and moves to the wounded part was recorded and analyzed every 6 hours for a total of 24 hours. The % wound area was calculated using **Equation 1**.

$$\frac{Wo}{Wt} * 100 = wound\ area\ (\%) \qquad \textbf{Equation 1}$$

Where:

Wo: measurement of wound area after creating a scratch,

Wt: measurement of wound area at time t.

Migration Assay

The migratory pattern assay identified the HDF cell's ability to migrate toward the conditioned samples (acts as a chemoattractant). 300 µL of 1.0X 10^6 cells/mL in serum-free media was added to the inside of the insert while 500 µL of conditioned samples were added to the lower well of the migration plate and incubated for 24 hours at 37°C and 5% CO_2 level. Media were aspirated from the

 doi:10.20944/preprints202506.0475.v1

inside of the insert, then transferred to a well with 225 µL cell detachment solution and incubated at 37°C for 30 minutes. The cells were dislodged from the underside of the membrane in the detachment solution and stained with 4X Lysis buffer/CyQuant®GR dye solution for 20 minutes at room temperature. Fluorescence was recorded with a fluorescence plate reader (BioTek Instruments, Inc., REF 800TS) set at 490 nm.

β-Galactosidase Staining

According to the manufacturer's protocol, a senescence cell histochemical staining kit (Sigma-Aldrich Cat. #CS0030-1KT) was used to measure the expression of β-galactosidase. Culturing human dermal fibroblast cells in the presence of conditioned nanocomposite fibers was followed by their fixation in 1X fixation buffer at room temperature for 6-7 minutes, staining the cells with the staining solution, and incubating the cells at 37°C overnight. The proportion of senescent cells (the fraction of cells expressing -galactosidase) was determined using the ratio of blue-stained cells.

In Vitro Drug Release Study

A previous protocol [36] was used to conduct the drug release study. In a 15 mL tube with 10 mL of PBS, 170–173 mg of gentamicin-loaded blown spun nanocomposite fibers were placed. The tubes were incubated with shaking at 37°C. Every 8 hours, 1 mL of the release solution from the tube was removed and replaced with the same volume of PBS. The release solution was examined using a plate reader (BioTek Instruments, Inc., REF 800TS) at 405 nm for 96 hours. Triplicates of each tube were created. The standard calibration curve was constructed by serially diluting a known gentamicin concentration.

Antimicrobial Testing

Drug Loading

Gentamicin sulfate was loaded into HNT using the vacuum entrapment method, which was later coated with MgO by electrodeposition process.

Kirby Bauer Disk Susceptibility Test

The zone diffusion assay, also known as the Kirby Bauer disk susceptibility test or the gentamicin sensitivity and resistance assay, was used to assess the impact of bacterial inhibition on blow-spun nanocomposite fibers. Bacteria cultures were let to reach an absorbance of 0.08 to 0.1 at 630 mm. *E. coli* and *S. aureus* were separately cultured with blown-spun nanocomposite fibers (5mm x 2mm) and covered in agar plates before being incubated at 37°C for 24 hours for *E. coli* and 18 hours for *S. aureus*. Commercially available gentamicin reference discs serve as a standard for the zone of inhibition when plated on agar plates.

Statistical Analysis

All results, unless otherwise stated, were presented as mean standard deviation (p 0.05, n = 3). Statistical analysis was carried out using Microsoft Excel and one-way analysis of variance (ANOVA) to ascertain differences between samples. As a result, a level of 0.05 or higher was regarded as statistically significant.

Results

Solvent Selection

Different solvents and their combination were used to determine the best combination for dissolving the polymers needed for fabrication, as shown in **Table 1**. Chloroform/acetone in 50:50

 doi:10.20944/preprints202506.0475.v1

proportion was chosen because acetone is FDA-approved, and the quantity of chloroform used evaporated within 24 hours, leaving the acetone.

Table 1. Solvent Selection Reaction.

Solvents	Reactions
Acetone	Did not dissolve.
Tetrahydrofuran (THF)	Did not dissolve.
Toluene	Did not dissolve.
Methyl ethyl ketone	Did not dissolve.
Chloroform	Dissolved overnight.
Dichloromethane	Dissolved overnight.
20%:80% Chloroform/acetone	Did not dissolve.
80%:20% Chloroform/acetone	Dissolved in 48 hours.
50%:50% Chloroform/acetone	Dissolved in 48 hours.
45%:55% Chloroform/acetone	Did not completely dissolve.

Material Characterization

Morphology and Surface Characterization of Blow-Spun Nanocomposite Fibers

Digital microscope images shown in Figure 2 show a uniform distribution of nanocomposites, but the SEM images shown in Figure 4 showed an uneven distribution of nanocomposites which is part of the limitation of SBS. The dark color observed in the images resulted from the presence of Si_3N_4. It can be seen in Figure 2F that the plain gauze has larger spaces which can result in larger pore size than the fibers with nanocomposites. The solvent dissolving the polymers evaporated after two days of fabrication, as evidenced in the preparation bottle. The analysis of HNT and MgO/HNT elements is shown in **Figure 3B**, which further confirms the electrodeposition process.

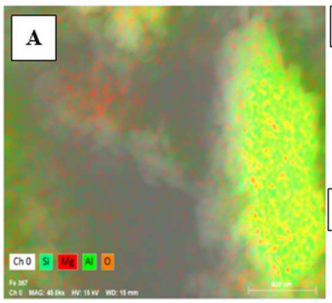

B

Element	At. No.	Netto	Mass [%]	Mass Norm. [%]	Atom [%]	abs. error [%] (1 sigma)	rel. error [%] (1 sigma)
Carbon	6	26172	68.38	68.38	76.49	8.55	12.51
Oxygen	8	4522	25.37	25.37	21.30	4.07	16.05
Gold	79	259	2.37	2.37	0.16	0.20	8.43
Magnesium	12	2375	2.22	2.22	1.23	0.17	7.45
Aluminium	13	1333	1.06	1.06	0.53	0.09	8.52
Silicon	14	1011	0.61	0.61	0.29	0.06	10.09
		Sum	100.00	100.00	100.00		

C

Element	At. No.	Netto	Mass [%]	Mass Norm. [%]	Atom [%]	abs. error [%] (1 sigma)	rel. error [%] (1 sigma)
Carbon	6	59478	72.39	72.39	78.73	8.45	11.67
Oxygen	8	8766	23.90	23.90	19.51	3.44	14.38
Aluminium	13	4317	1.93	1.93	0.94	0.12	6.43
Silicon	14	3905	1.78	1.78	0.83	0.11	6.11
		Sum	100.00	100.00	100.00		

Figure 2. Digital microscope images of surface morphology of (A) 25% Si_3N_4/PLA Fiber (B) 30% Si_3N_4/PLA Fiber (C) 25% Si_3N_4/MgHNT/PLA Fiber (D) 25% MgHNT/PLA Fiber (E) 30% Si_3N_4/MgHNT/PLA Fiber (F) plain gauze lacking inclusion of the nanocomposite.

 doi:10.20944/preprints202506.0475.v1

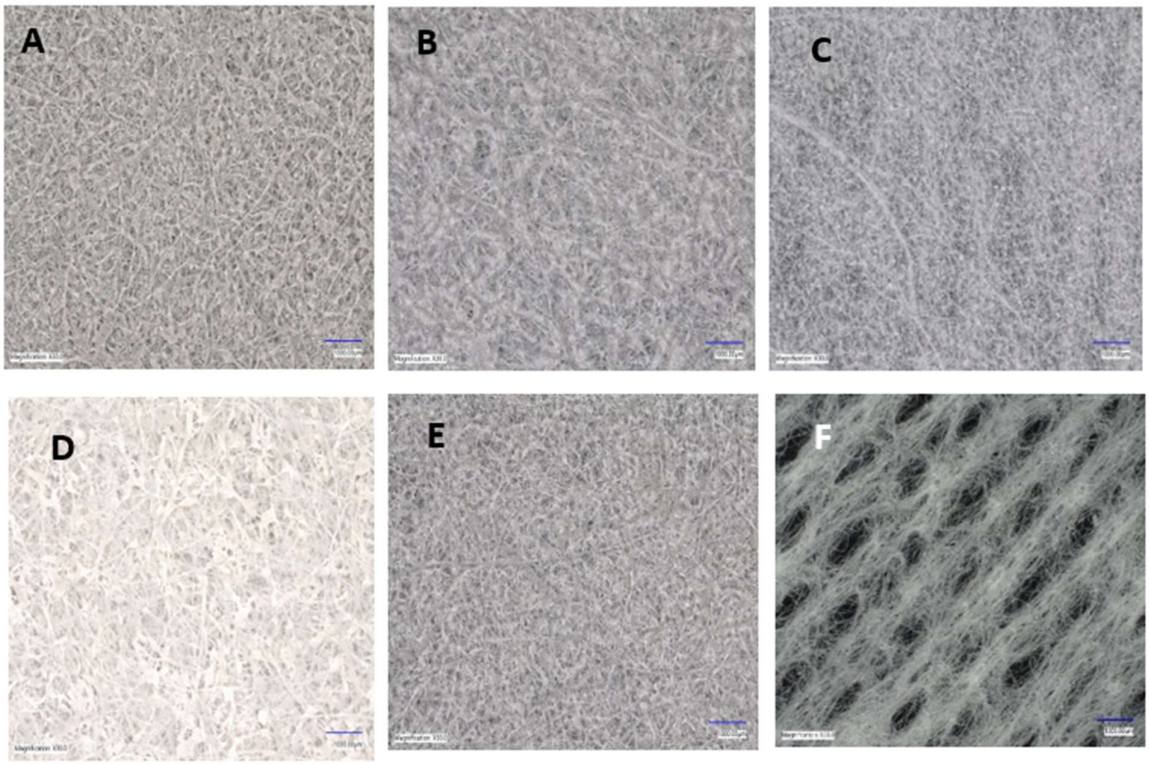

Figure 3. (A) Energy Dispersive X-ray Spectroscopy Scan (B) Chemical element analysis of MgO/HNT confirming the presence of Mg. (C) Chemical element analysis of HNT confirming the absence of Mg. .

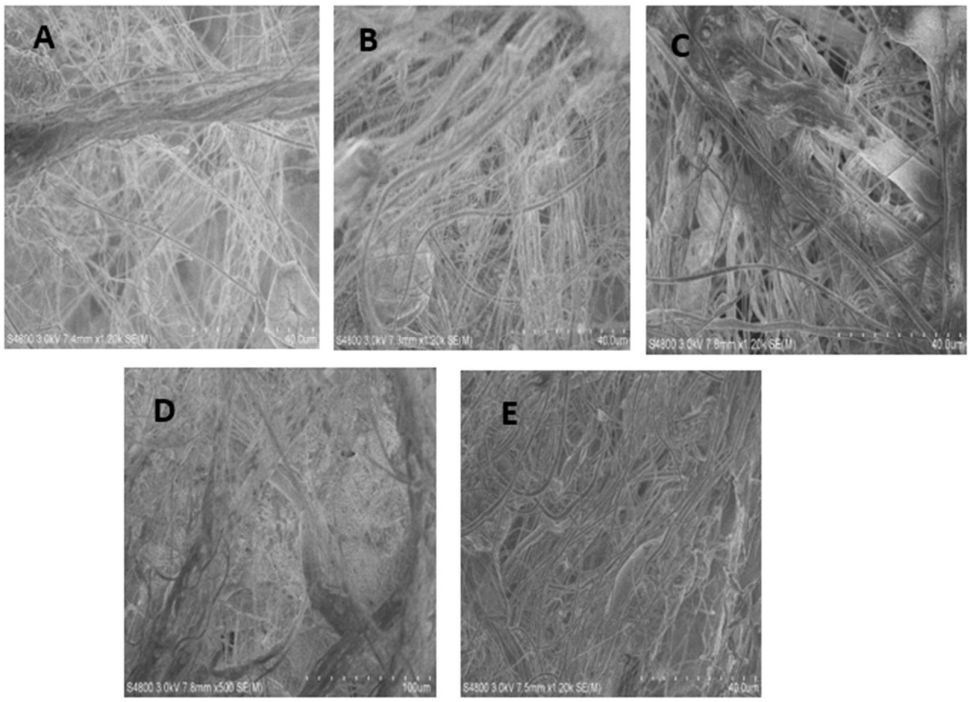

Figure 4. SEM images of surface morphology of (A) 25% Si_3N_4/PLA Fiber (B) 25% MgHNT/PLA Fiber (C) 25% Si_3N_4/MgHNT/PLA Fiber (D) 30% Si_3N_4/PLA Fiber (E) 30% Si_3N_4/MgHNT/PLA Fiber.

 doi:10.20944/preprints202506.0475.v1

In Vitro Fibroblast Response

Cell Proliferation Assay Test

Confirming that the blow-spun nanocomposite fibers will not hinder human dermal fibroblast cell proliferation is necessary. Therefore, a proliferation assay on the fibers was performed for 7 days, as shown in Figure 5. 25% and 30% MgO/HNT/PLA fibers have the lowest proliferation rate compared to other nanocomposite fibers. Surprisingly, Si_3N_4/MgO/HNT/PLA fibers proliferated better than Si_3N_4/PLA fibers since the total composition of Si_3N_4 (which aids proliferation rate) in Si_3N_4/PLA fibers double the Si_3N_4 in Si_3N_4/MgO/HNT/PLA. It was observed that the proliferation rate of control cells dropped after day 5; however, 30% nanocomposite fibers proliferated more than 25% nanocomposite fibers.

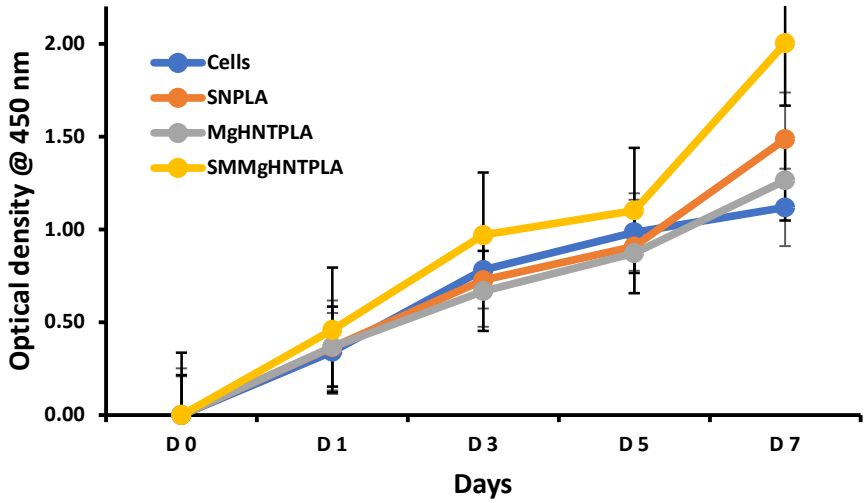

Figure 5. Proliferation assay of blow spun nanocomposite fiber after exposure to human Dermal Fibroblast for 7 days. The Blue Line Signified Control Cells. Yellow, Orange, and Grey Lines Signify Si_3N_4MgO/HNT/PLA, Si_3N_4/PLA, and MgO/HNT/PLA, respectively. Error bars are standard deviations, where n = 3.

Cytotoxicity Assay Test

Control cells are cells without the samples, which act as a negative control. Control cells at the beginning of day 1 have a viability percentage of approximately 97.5% and increased to 98.1% at the end of day 7. 25% Si_3N_4PLA fibers at the beginning of day 1 have a viability percentage of approximately 94.9% and 98.6% at the end of day 7. Additionally, 25% MgO/HNT/PLA fibers dropped from 94.9% on day 1 to 91.2% on day 3, then increased to 94.6% on day 7. Similarly, 25% Si_3N_4MgO/HNTPLA fibers increased in percent viability from 94.9% on day 1 to 95.8% on day 5, then decreased to 95.2% on day 7. However, 30% Si_3N_4MgO/HNTPLA fibers have the highest viability percentage, from 86.5% on day 1 to 98.4% on day 7. All nanocomposites have a higher or slightly lower percent cell viability difference of 0.15. The images of the live and dead cells are shown in Figure 6. Graphs showing quantitative values of calculated cell count are shown in Figure 7.

 doi:10.20944/preprints202506.0475.v1

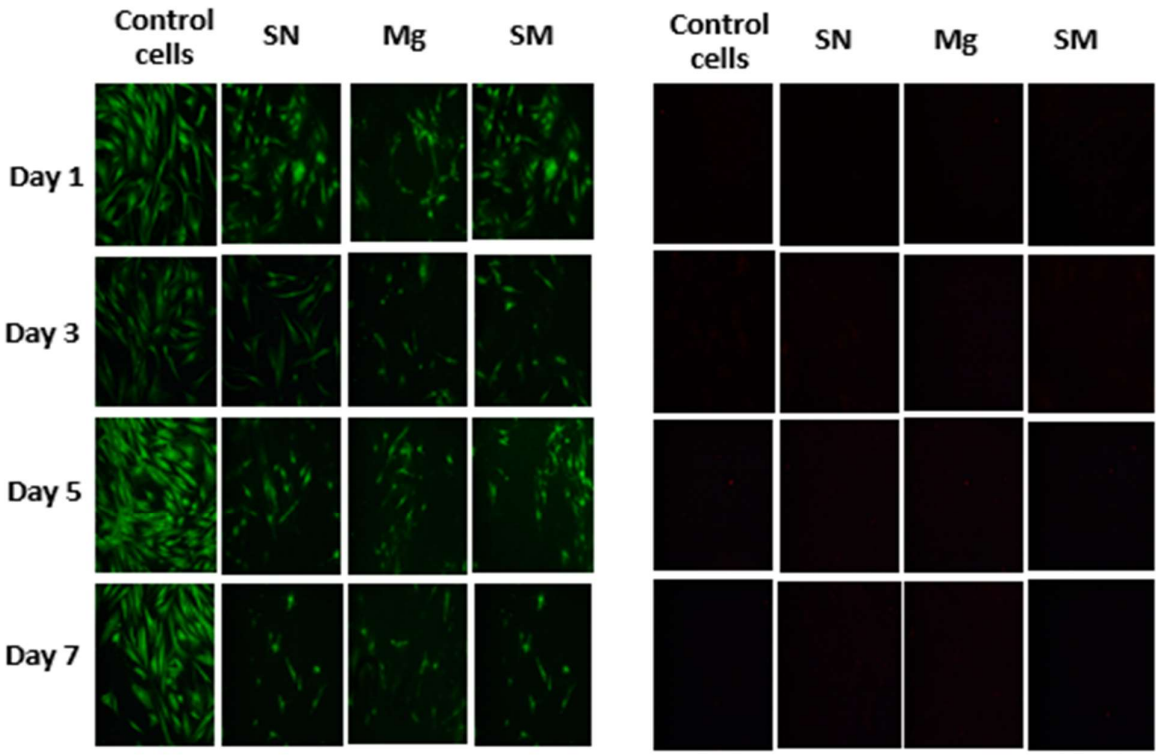

Figure 6. Images of Cytotoxicity Test (Live/Dead Assay) with Human Dermal Fibroblast Cell of Blow Spun Nanocomposite Fibers. Live Cells in Green (Left Image) and Dead Cells in Red or Black Indicate no Dead Cell (Right Image) for Day 1, 3, 5, and 7; SN = Si_3N_4/PLA, Mg = MgO/HNT/PLA, SM = Si_3N_4MgO/HNT/PLA.

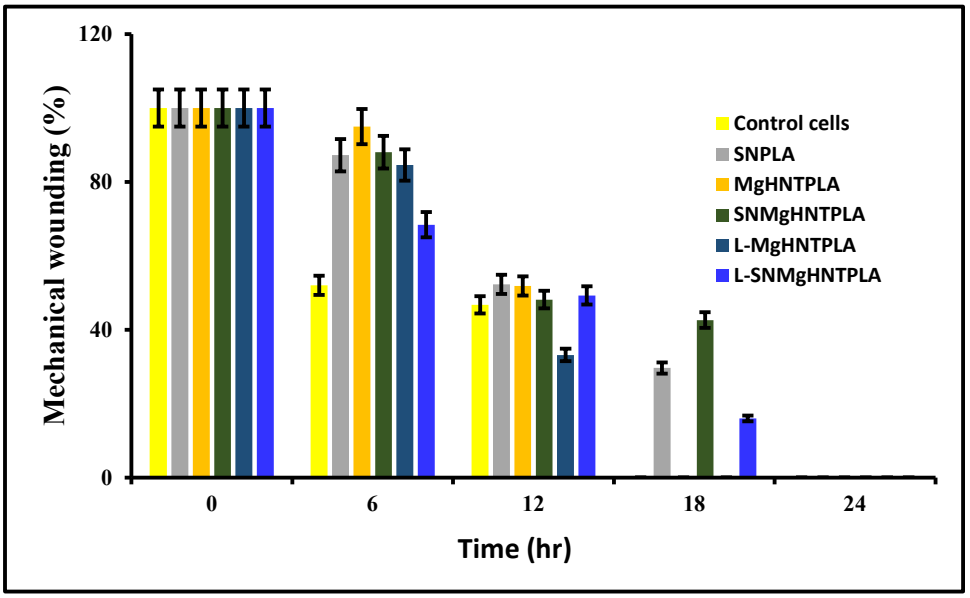

Figure 7. Viability on Blow Spun Nanocomposite Fibers Showing Quantitative Cell Count Value Calculated (Live Cells/Total Cell Count). Error Bars are Standard Deviations, where n = 3.

Scratch Assay

The behavior of human dermal fibroblast cells in the scratch assay is shown in Figure 9, while the quantification is shown in Figure 8. Control cells, MgO/HNT/PLA fibers, and L-MgO/HNT/PLA

 doi:10.20944/preprints202506.0475.v1

fibers all showed cells in the wounded part migrated and closed the gap after 18 hours, and all nanocomposite fibers showed 100% wound closure after 24 hours. Although irregular scratches when making manual wounding is one of the disadvantages of the scratch assay, this can also lead to the destruction of cell culture plate coating if not properly done.

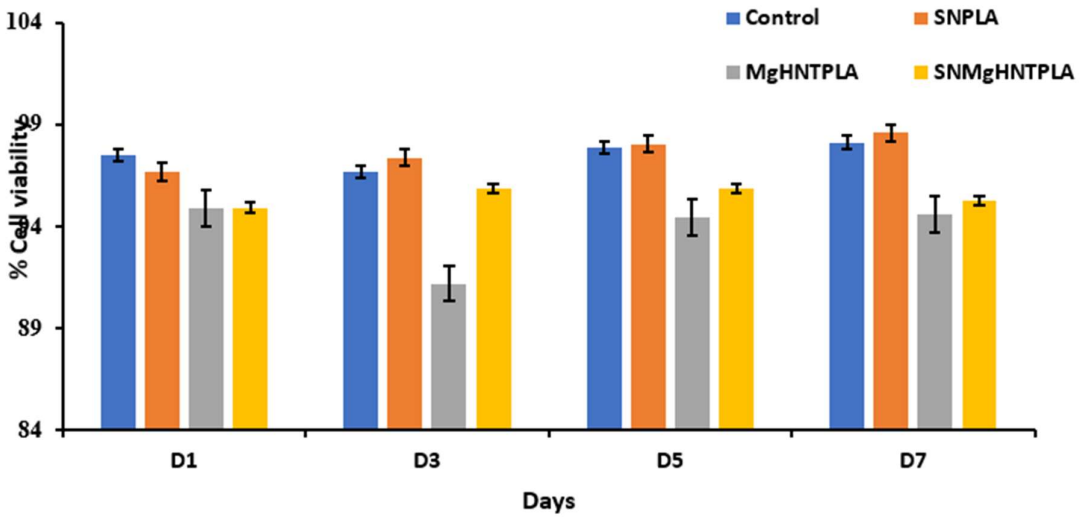

Figure 8. Scratch assay quantification of blow-spun nanocomposite fibers. Error Bars are standard deviations where n = 3.

 doi:10.20944/preprints202506.0475.v1

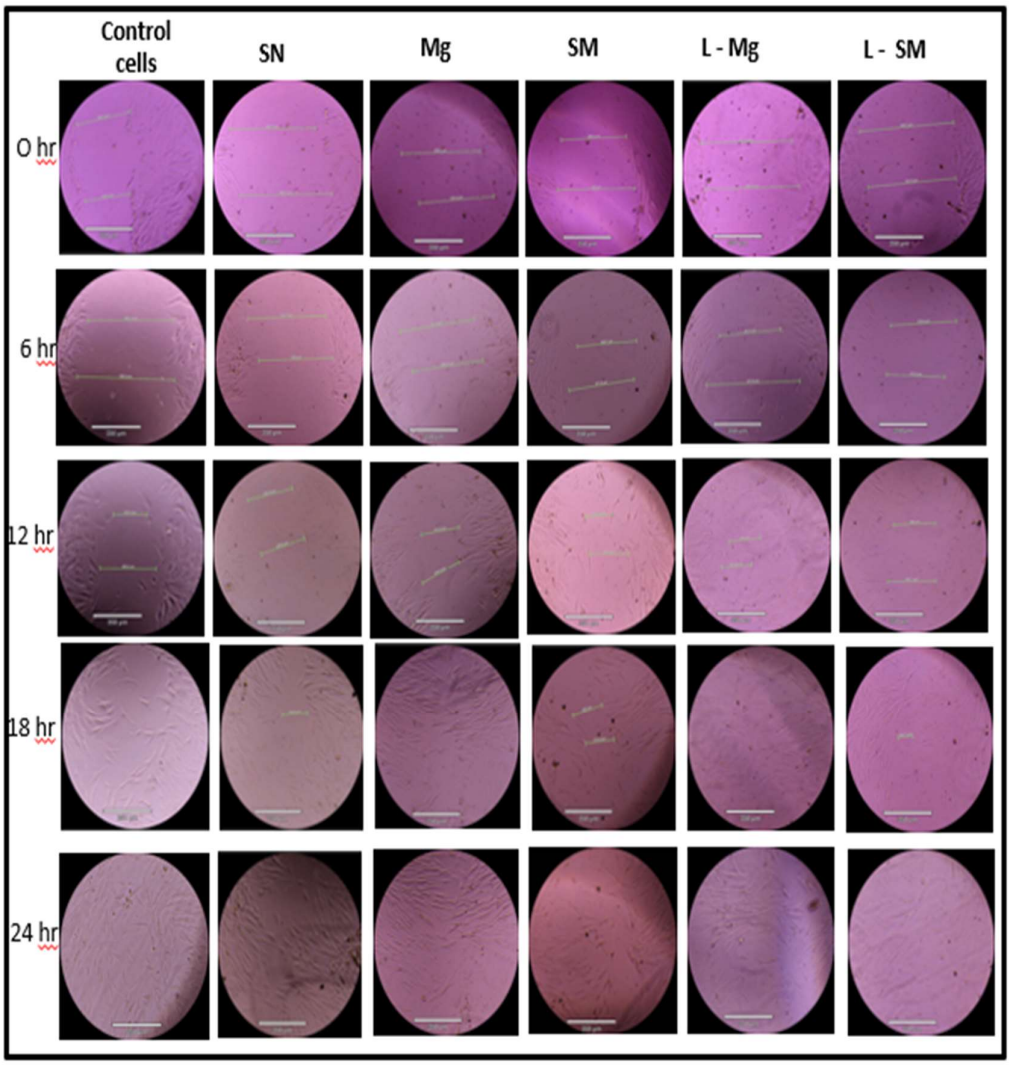

Figure 9. Images of Mechanical Wound Assay (Scratch Assay) with Human Dermal Fibroblast Cell of Blow Spun Nanocomposite Fibers for 0 hour, 6 hour, 12 hour, 18 hour, and 24 hour. Control Cells are without the Nanocomposites, SN = Si_3N_4/PLA, Mg = MgO/HNT/PLA, SM = Si_3N_4MgO/HNT/PLA, L-Mg = Gentamicin Loaded MgO/HNT/PLA, and L-SM = Gentamicin Loaded Si_3N_4MgO/HNT/PLA.

Migration Assay

The migratory analysis is characterized in Figure 10. Negative control cells (human dermal fibroblast cells) show a decrease in cell migration which was expected due to the absence of nanocomposites acting as a chemoattractant. 25% and 30% Si_3N_4PLA show the highest overall rise in cell migration through the chamber pore. All nanocomposite fibers show an increase in cell migration except for the 25% MgO/HNTPLA fibers showing an approximately equal cell migration as the positive control cells.

 doi:10.20944/preprints202506.0475.v1

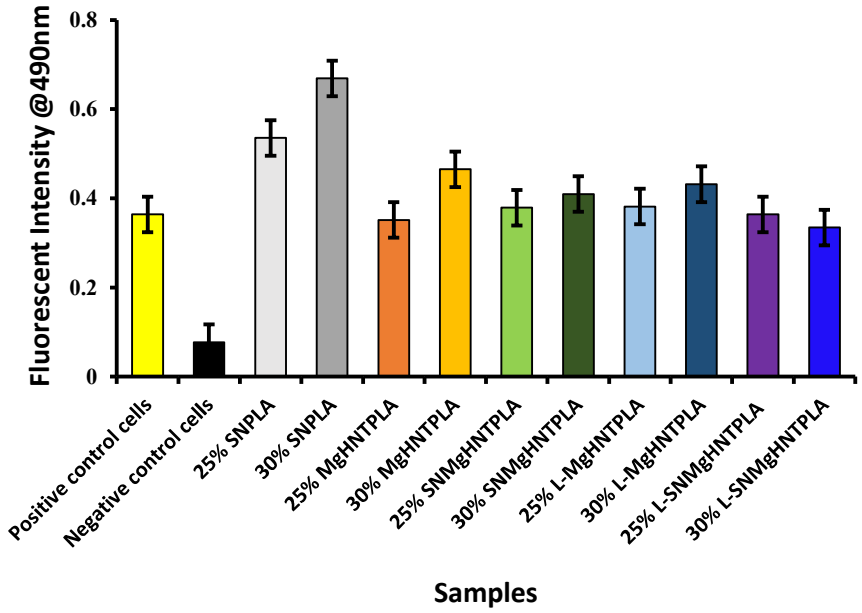

Figure 10. Graphical Representation of Cell Migration Assay of Blow-Spun Nanocomposite Fibers with Human Dermal Fibroblast Cells. Error Bars are Standard Deviations, where n = 3.

β-Galactosidase Staining

Images of SA-β-galactosidase-stained human dermal fibroblast cells are shown in **Figure 11,** and the percentage of the SA-β-galactosidase-stained positive cells is shown in **Figure 12**. All 25% nanocomposites fibers showed a low percentage of β-galactosidase positive cells (0.005% and below) compared to the 30% nanocomposites and the control cells, indicating low signs of senescence except the 25% Si_3N_4PLA showing around 0.05%.

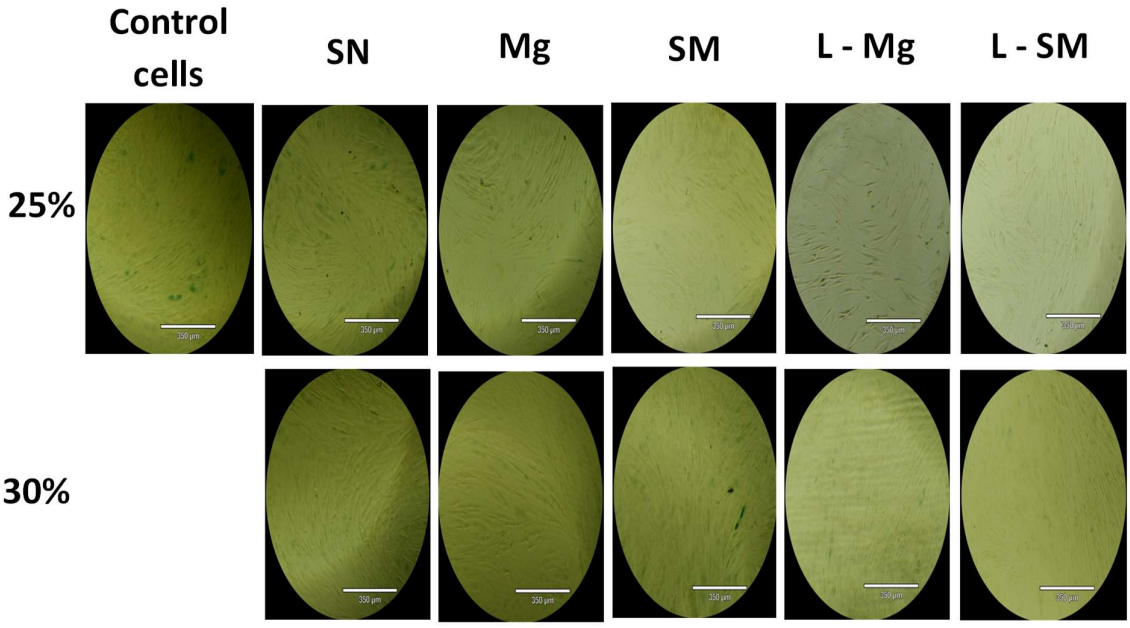

Figure 11. Images of β-Galactosidase Test with Human Dermal Fibroblast Cell of 25% and 30% Blow-Spun Nanocomposite Fibers. Control Cells are without the Nanocomposites, SN = Si_3N_4/PLA, Mg = MgO/HNT/PLA,

 doi:10.20944/preprints202506.0475.v1

SM = Si_3N_4MgO/HNT/PLA, L-Mg = Gentamicin Loaded MgO/HNT/PLA, and L-SM = Gentamicin Loaded Si_3N_4MgO/HNT/PLA.

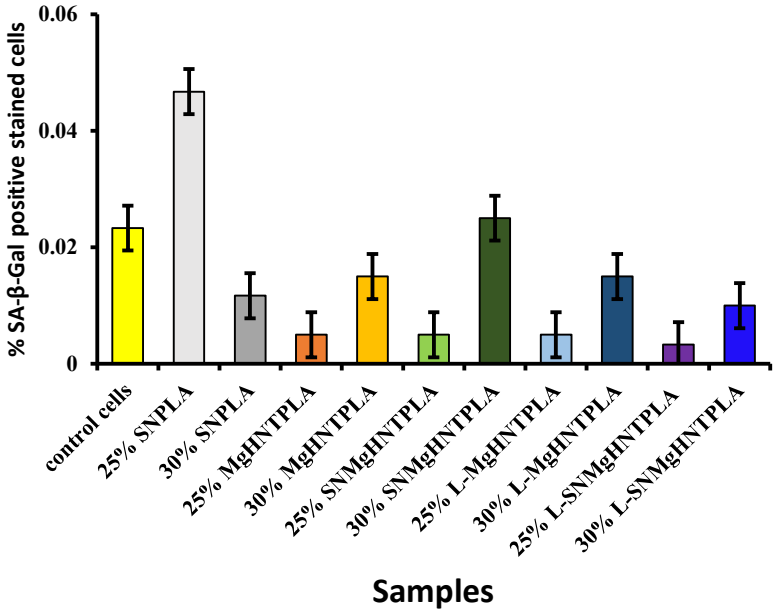

Figure 12. Graphical representation of % SA-β-Gal Positive Stained Cells of Blow-Spun Nanocomposite Fibers with Human Dermal Fibroblast Cells. Error Bars are Standard Deviations, where n = 3.

In Vitro Drug Release Study

The percentage of drug release from gentamicin-loaded nanocomposites is shown in Figure 13. There was a burst release at the beginning of the experiment, around 8 hours, followed by a more constant, stable release rate until 64 hours, where it bursts out again before retaining the stable release. However, most of the nanocomposites followed a mono-phasic kinetics where controlled release is at a more stable and constant rate.

 doi:10.20944/preprints202506.0475.v1

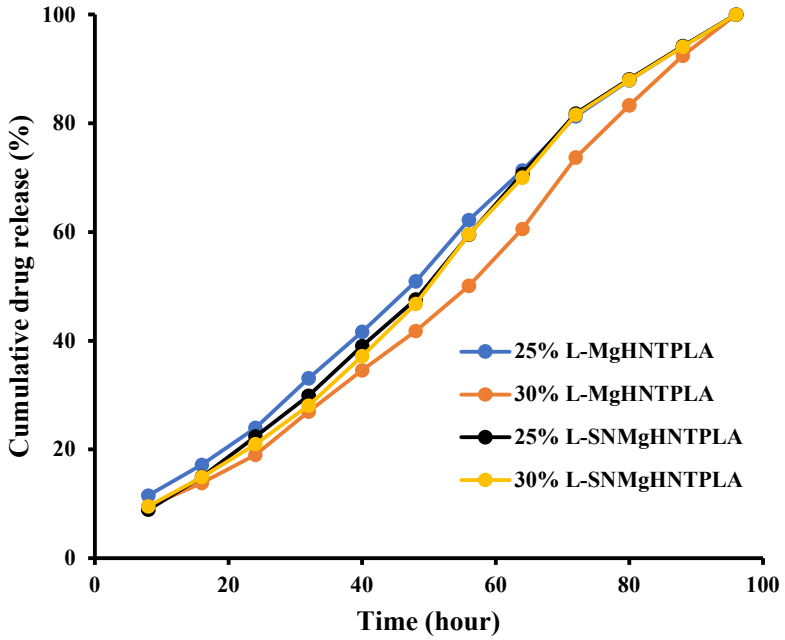

Figure 13. In Vitro Cumulative Release of Gentamicin from Blow-Spun Nanocomposite Fibers to PBS Buffer Solution at 37°C.

Antimicrobial Testing of Blow-Spun Nanocomposite Fibers

Kirby Bauer Disk Susceptibility Test

The zone of inhibition was measured in centimeters and plotted. The image of the inhibition zone against *E. coli* is shown in Figure 14, while that of *S. aureus* is shown in Figure 16. The graphical representation of the inhibition zone against *E. coli* is shown in Figure 15, while that of *S. aureus* is shown in Figure 17. The standard gentamicin disc showed an increased zone of inhibition after 24 hours for *E. coli* and 18 hours for *S. aureus*. However, all other sample groups showed reduced bacteria inhibition, with the least effective being the 30% MgO/HNTPLA fiber for both *E. coli* and *S. aureus*.

 doi:10.20944/preprints202506.0475.v1

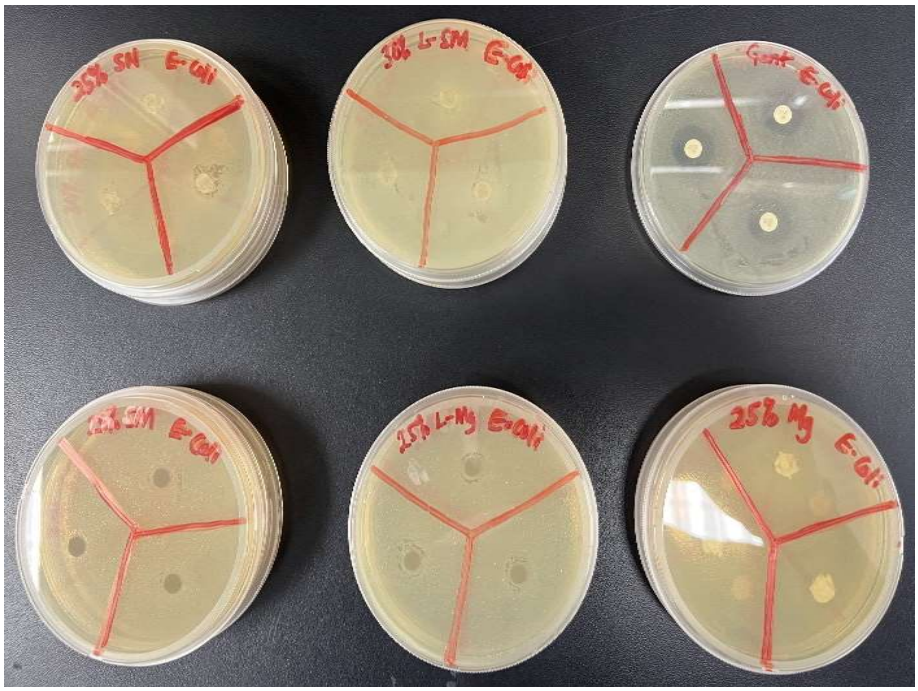

Figure 14. Image of Bacteria Culture Plates, with *E. coli* and (A) Si_3N_4/PLA Fiber (B) L-$S_{3i}N_4$MgO/HNT/PLA Fiber (C) Gentamicin Standard Disc (D) Si_3N_4MgO/HNT/PLA Fiber (E) L-MgO/HNT/PLA Fiber (F) MgO/HNT/PLA Fiber.

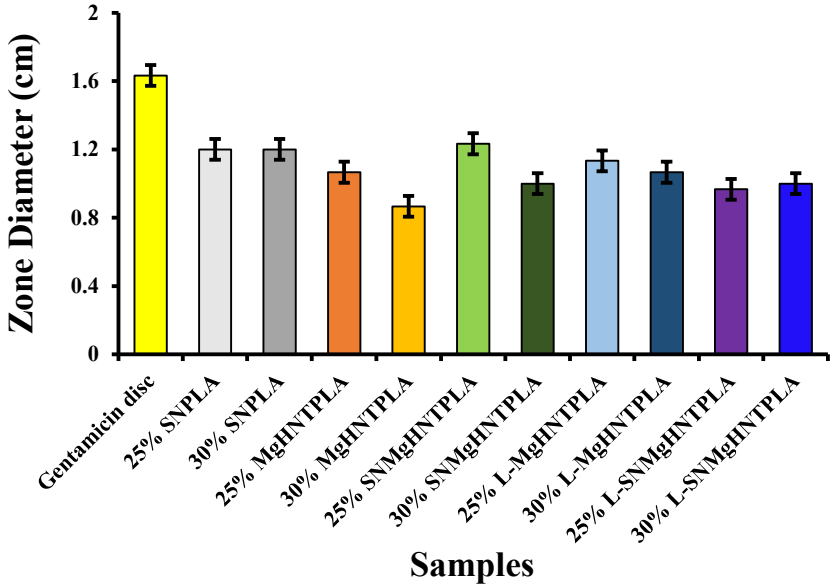

Figure 15. Graphical Representation of Zone Diffusion Assay of Blow-Spun Nanocomposite Fibers Against *E. coli.* Error Bars are Standard Deviations where n = 3.

 doi:10.20944/preprints202506.0475.v1

Figure 16. Image of bacteria culture plates, with *S. aureus* and (A) Si_3N_4MgO/HNT/PLA Fiber (B) Si_3N_4/PLA Fiber (C) L-Si_3N_4MgO/HNT/PLA Fiber (D) MgO/HNT/PLA Fiber (E) L-MgO/HNT/PLA Fiber (F) Gentamicin standard disc.

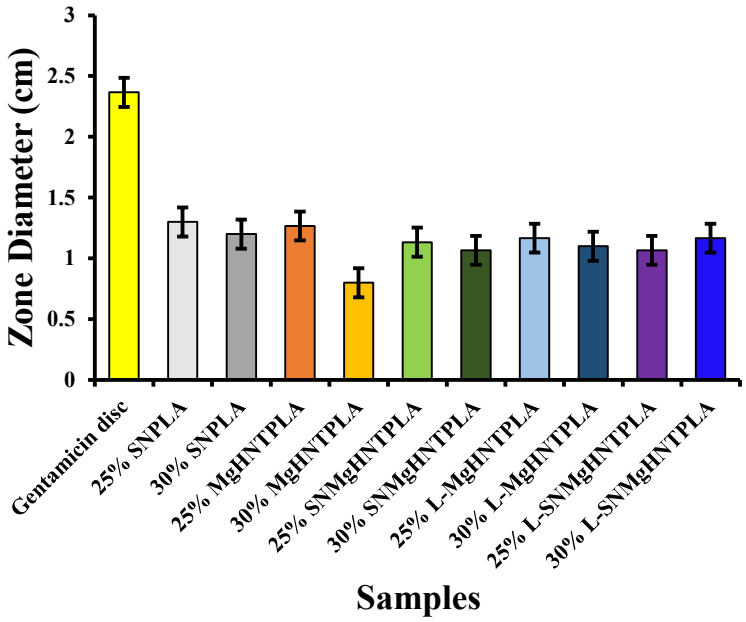

Figure 17. Graphical Representation of Zone Diffusion Assay of Blow-Spun Nanocomposite against *S. aureus*. Error Bars are Standard Deviations, where n = 3.

Discussion

The most widely used wound healing material, plain gauze in wound dressing, tends to coagulate and reduce bleeding without advancing the wound healing process [37]. A hemorrhage is a critical cause of civilian and military casualties. The human body's hemostatic mechanism is a complex process with a limited capacity [38]. In critical emergencies, the human hemostatic mechanism cannot stop bleeding effectively, and hemostatic materials are needed to save lives. The most commonly used hemostatic materials (including fibrin, collagen, zeolite, gelatin, alginate, chitosan, cellulose, and cyanoacrylate) and commercial wound dressings[40].

 doi:10.20944/preprints202506.0475.v1

The Committee on Tactical Combat Casualty Care (CoTCCC) has recently recommended QuickClot combat gauze® (QCG), a material containing either Kaolin or Zeolite – to control bleeding in the military [39]. Hematrix® an active-patch wound dressing for immediate hemostasis, is another widely used hemostatic material. These materials may have limitations, such as poor tissue adhesion, infection risk, exothermic reactions, and no regenerative capability that may lessen their efficacy and cause secondary injuries [38,40]. Therefore, there is a need to improve the current wound healing capability by incorporating additional properties needed for wound healing, eliminating infection without using drugs, enhancing trauma site recovery, tissue regenerative, and drug release capability. Multifunctional bandages (antimicrobial, pain relief, and regenerative) could be effective for wound repair and regeneration.

Halloysite has been studied as a delivery vehicle for wound healing applications [41,32]. Halloysite coupled with antimicrobial metals such as gold [43], silver [44] and zinc [45]. Halloysite and chitosan have been studied for their antimicrobial and hemostatic capability [46]. Chitosan's inherent antimicrobial property [46] was combined with halloysite ability as an absorbent to create antimicrobial and hemostatic bandages [47,48] and often combined with various drugs to enhance the bandages efficacy [41,42,49].

This research aimed to produce novel gauze dressing using commercial gauze (with large openings) as the base material, with advanced nanocomposites, adding additional functionalities to current wound dressings. Figure 2 shows plain gauze having a large opening and lacking good coagulation capability.

Here, our approach in fabricating an antimicrobial and tissue regenerative bandage was through the combination of MgO/HNTs doped with gentamicin and included in solution spun fibers. FDA-approved materials like PLA, Si_3N_4, MgO, HNT, and suitable solvents were used to fabricate nanocomposite fibers. HNT is a clay material, just like Kaolin or Zeolite. Therefore, the solvents used in dissolving the polymers required for fabrication are an essential part of the fabrication process. Since chloroform/acetone in the ratio 45:55 does not dissolve the polymers completely, there was a need to make the ratio equal, that is, a 50:50 ratio. Fortunately, chloroform or dichloromethane evaporates after 24 hours, leaving the acetone. As stated earlier, the high evaporation rate in SBS is one of the advantages over other spinning techniques.

Cell proliferation is essential in the treatment of wounds. The proliferation assay on the nanocomposite fibers indicated that all nanocomposite fibers proliferated well, especially the Si_3N_4MgO/HNT/PLA and Si_3N_4PLA, due to the presence of Si_3N_4, making them proliferate better than the control cells and other nanocomposites fibers without Si_3N_4. Wound dressing must not be toxic to cells because cell growth is essential in treating wounds. Furthermore, the cytotoxicity tests showed that the nanocomposite fibers were not toxic, making their application in wound healing viable.

Since cytotoxicity and the proliferation rate has been established, it is essential to know how the nanocomposite fibers will behave in vitro. The mechanical wounding process, also known as the scratch assay in **Figures 8** and **9,** shows that the cells in the wounded part migrated toward the gap in the presence of the nanocomposite fibers. It was discovered that 30% of gentamicin-loaded MgO/HNT/PLA fibers saw cells migrated and covered the wounded surface within 18 hours, while all other 30% nanocomposites covered the wounded surface by 24 hours. However, the control cells, 25% MgO/HNT/PLA, and 25% gentamicin-loaded MgO/HNT/PLA fibers were also covered in 18 hours, but all other 25% nanocomposite fibers were covered in 24 hours.

The nanocomposite fibers were used as a chemoattractant in the migration assay to determine how the cells would migrate toward the nanocomposites. **Figure 10** showed that all nanocomposite fibers had increased cell migration. Similarly, the phase contrast images of β-galactosidase-stained human dermal fibroblast cells and their respective percentages were shown in **Figures 11 and 12,** indicating that all 25% nanocomposite fibers showed a low percentage of positive SA-β-galactosidase cells around 0.005% and below while the control cells also showing low signs of senescence but higher than the 25% nanocomposite fibers.

 doi:10.20944/preprints202506.0475.v1

The drug delivery capability is one of the improved properties expected in the nanocomposites incorporated in wound dressing. Therefore, gentamicin was loaded into the nanocomposite fibers by vacuum entrapment method and subjected to an in vitro drug release study in the presence of PBS. The results shown in **Figure 13** indicated that most nanocomposites released the drug at a more stable and constant rate.

Antimicrobial activities of the nanocomposite fibers suppressed bacterial growth at a lower rate within 24 hours when tested against *E. coli* and *S. aureus*. However, the gentamicin reference disc performed excellently in suppressing bacterial growth. The analysis of the bacteria test shown in Figures 14, 15, 16, and 17 showed how the reference disc performed better. All nanocomposite fibers performed similarly against *E. coli* and *S. aureus* except 30% MgO/HNTPLA which performed less.

Conclusions

Fabricated fiber-containing Si_3N_4/Mg/HNT/PLA/chloroform: acetone showed excellent prospects when compared to fabricated Mg/HNT/PLA/chloroform: acetone fiber and Si_3N_4/PLA/chloroform: acetone fiber because each component brought significant advantages to the fiber, such as inherent antimicrobial properties that can reduce the spread of infection and able to support the growth and collagen formation in biological systems, biodegradability, favorable mechanical properties and they are eco-friendly and low-cost materials. Our favorable results suggest that our composite fiber may have multifunctional applications in biomedical use as a wound dressing material to reduce microbial infection, enhance wound healing, and be used for drug delivery.

However, using nanocomposites may prove superior since bio-zeolite gauze has already proved superior to QCG.

References

1. Agarwal S, Krishnamurthy K. Histology, Skin. StatPearls. Published online 2019. Accessed May 5, 2023. http://www.ncbi.nlm.nih.gov/pubmed/30726010
2. Ranghar S, Sirohi P, Verma P, Agarwal V. Nanoparticle-based drug delivery systems: promising approaches against infections. Brazilian Arch Biol Technol. 2013;57(2):209-222. doi:10.1590/S1516-89132013005000011
3. Järbrink K, Ni G, Sönnergren H, et al. Prevalence and incidence of chronic wounds and related complications: a protocol for a systematic review. Syst Rev. 2016;5(1). doi:10.1186/S13643-016-0329-Y
4. Simões D, Miguel SP, Ribeiro MP, Coutinho P, Mendonça AG, Correia IJ. Recent advances on antimicrobial wound dressing: A review. Eur J Pharm Biopharm. 2018;127:130-141. doi:10.1016/J.EJPB.2018.02.022
5. Kubíčková J, Medek T, Husby J, et al. Nonwoven Textiles from Hyaluronan for Wound Healing Applications. Biomolecules. 2021;12(1). doi:10.3390/BIOM12010016
6. Faris Taufeq FY, Habideen NH, Rao LN, Podder PK, Katas H. Potential Hemostatic and Wound Healing Effects of Thermoresponsive Wound Dressing Gel Loaded with Lignosus rhinocerotis and Punica granatum Extracts. Gels (Basel, Switzerland). 2023;9(1). doi:10.3390/gels9010048
7. Zhang Y, Demir B, Bertsch G, Qiao M. Zwitterion and N-halamine functionalized cotton wound dressing with enhanced antifouling, antibacterial, and hemostatic properties. Int J Biol Macromol. 2023;230. doi:10.1016/j.ijbiomac.2022.123121
8. Gong F, Yang N, Xu J, et al. Calcium Hydride-Based Dressing to Promote Wound Healing. Adv Healthc Mater. 2023;12(2). doi:10.1002/adhm.202201771
9. Zhang T, Guo L, Li R, et al. Ellagic Acid-Cyclodextrin Inclusion Complex-Loaded Thiol-Ene Hydrogel with Antioxidant, Antibacterial, and Anti-inflammatory Properties for Wound Healing. ACS Appl Mater Interfaces. 2023;15(4):4959-4972. doi:10.1021/acsami.2c20229
10. Kavousi Heidari M, Pourmadadi M, Yazdian F, et al. Wound dressing based on PVA nanofiber containing silk fibroin modified with GO/ZnO nanoparticles for superficial wound healing: In vitro and in vivo evaluations. Biotechnol Prog. Published online February 8, 2023:e3331. doi:10.1002/btpr.3331

 doi:10.20944/preprints202506.0475.v1

11. Weng P, Liu K, Yuan M, et al. Development of a ZIF-91-Porous-Liquid-Based Composite Hydrogel Dressing System for Diabetic Wound Healing. Small. Published online March 18, 2023:e2301012. doi:10.1002/smll.202301012
12. Elsherbiny DA, Abdelgawad AM, Shaheen TI, Abdelwahed NAM, Jockenhoevel S, Ghazanfari S. Thermoresponsive nanofibers loaded with antimicrobial α-aminophosphonate-o/w emulsion supported by cellulose nanocrystals for smart wound care patches. Int J Biol Macromol. 2023;233. doi:10.1016/J.IJBIOMAC.2023.123655
13. Chen G, Hu J, Hong Z, et al. Multifunctional Electrospun Textiles for Wound Healing. J Biomed Nanotechnol. 2022;18(3):796-806. doi:10.1166/JBN.2022.3288
14. Uhljar LÉ, Ambrus R. Electrospinning of Potential Medical Devices (Wound Dressings, Tissue Engineering Scaffolds, Face Masks) and Their Regulatory Approach. Pharmaceutics. 2023;15(2). doi:10.3390/pharmaceutics15020417
15. Scaffaro R, Settanni L, Gulino EF. Release Profiles of Carvacrol or Chlorhexidine of PLA/Graphene Nanoplatelets Membranes Prepared Using Electrospinning and Solution Blow Spinning: A Comparative Study. Molecules. 2023;28(4). doi:10.3390/molecules28041967
16. Bang J, Park S, Hwang SW, et al. Biodegradable and hydrophobic nanofibrous membranes produced by solution blow spinning for efficient oil/water separation. Chemosphere. 2023;312. doi:10.1016/j.chemosphere.2022.137240
17. Daristotle JL, Behrens AM, Sandler AD, Kofinas P. A Review of the Fundamental Principles and Applications of Solution Blow Spinning. Vol 8.; 2016. doi:10.1021/acsami.6b12994
18. Gao Y, Zhang J, Su Y, et al. Recent progress and challenges in solution blow spinning. Mater Horizons. 2021;8(2):426-446. doi:10.1039/d0mh01096k
19. Lou H, Li W, Li C, Wang X. Systematic investigation on parameters of solution blown micro/nanofibers using response surface methodology based on box-Behnken design. J Appl Polym Sci. 2013;130(2):1383-1391. doi:10.1002/app.39317
20. Rai M, Shegokar R. Metal nanoparticles in pharma. Met Nanoparticles Pharma. Published online 2017:1-493. doi:10.1007/978-3-319-63790-7
21. Swaminathan M, Sharma NK. Antimicrobial Activity of the Engineered Nanoparticles Used as Coating Agents. Handb Ecomater. Published online 2018:1-15. doi:10.1007/978-3-319-48281-1_1-1
22. Yaghubi kalurazi T, Jafari A. Evaluation of magnesium oxide and zinc oxide nanoparticles against multi-drug-resistance Mycobacterium tuberculosis. Indian J Tuberc. 2021;68(2):195-200. doi:10.1016/J.IJTB.2020.07.032
23. Staroń A, Długosz O. Antimicrobial properties of nanoparticles in the context of advantages and potential risks of their use. J Environ Sci Heal - Part A Toxic/Hazardous Subst Environ Eng. 2021;56(6):680-693. doi:10.1080/10934529.2021.1917936
24. Pezzotti G, Bock RM, Adachi T, et al. Silicon nitride surface chemistry: A potent regulator of mesenchymal progenitor cell activity in bone formation. Appl Mater Today. 2017;9:82-95. doi:10.1016/j.apmt.2017.05.005
25. Pezzotti G, McEntire BJ, Bock R, et al. Silicon Nitride: A Synthetic Mineral for Vertebrate Biology. Sci Rep. 2016;6:2-8. doi:10.1038/srep31717
26. Pezzotti G, Marin E, Adachi T, et al. Bioactive silicon nitride: A new therapeutic material for osteoarthropathy. Sci Rep. 2017;7(February):1-11. doi:10.1038/srep44848
27. Pezzotti, Marin, Zanocco, et al. Osteogenic Enhancement of Zirconia-Toughened Alumina with Silicon Nitride and Bioglass®. Ceramics. 2019;2(4):554-567. doi:10.3390/ceramics2040043
28. Yunsheng D, Hui X, Jie W, et al. Sustained release silicon from 3D bioprinting scaffold using silk/gelatin inks to promote osteogenesis. Int J Biol Macromol. 2023;234. doi:10.1016/j.ijbiomac.2023.123659
29. Dai Y, Guo H, Chu L, et al. Promoting osteoblasts responses in vitro and improving osteointegration in vivo through bioactive coating of nanosilicon nitride on polyetheretherketone. J Orthop Transl. 2020;24:198-208. doi:10.1016/j.jot.2019.10.011
30. Machowska A, Klara J, Ledwójcik G, Wójcik K, Dulińska-Litewka J, Karewicz A. Clindamycin-Loaded Halloysite Nanotubes as the Antibacterial Component of Composite Hydrogel for Bone Repair. Polymers (Basel). 2022;14(23). doi:10.3390/POLYM14235151

 doi:10.20944/preprints202506.0475.v1

31. Bal BS, Khandkar A, Lakshminarayanan R, Clarke I, Hoffman AA, Rahaman MN. Fabrication and Testing of Silicon Nitride Bearings in Total Hip Arthroplasty. Winner of the 2007 "HAP" PAUL Award. J Arthroplasty. 2009;24(1):110-116. doi:10.1016/j.arth.2008.01.300
32. Satish S, Tharmavaram M, Rawtani D. Halloysite nanotubes as a nature's boon for biomedical applications. BJGP Open. 2019;6:1-16. doi:10.1177/1849543519863625
33. Fakhruddin K, Hassan R, Khan MUA, et al. Halloysite nanotubes and halloysite-based composites for biomedical applications. Arab J Chem. 2021;14(9):103294. doi:10.1016/j.arabjc.2021.103294
34. Wu K, Feng R, Jiao Y, Zhou C. Effect of halloysite nanotubes on the structure and function of important multiple blood components. Mater Sci Eng C. 2017;75:72-78. doi:10.1016/j.msec.2017.02.022
35. Yang Y, Chen Y, Leng F, Huang L, Wang Z, Tian W. Recent advances on surface modification of halloysite nanotubes for multifunctional applications. Appl Sci. 2017;7(12). doi:10.3390/app7121215
36. Wu J, Xu S, Han CC, Yuan G. Controlled drug release: On the evolution of physically entrapped drug inside the electrospun poly(lactic-co-glycolic acid) matrix. J Control Release. 2021;331(October 2020):472-479. doi:10.1016/j.jconrel.2021.01.038
37. 37. Sheokand, B., Vats, M., Kumar, A., Srivastava, C. M., Bahadur, I., & Pathak, S. R. Natural polymers used in the dressing materials for wound healing: Past, present and future. J. Poly Sci. https://doi.org/10.1002/pol.20220734
38. Jia Y jun, Du W qiong, Zong Z wen, et al. Hemostatic Effects of Bio-Zeolite Gauze and QuikClot Combat Gauze on Major Bleeding in Rabbits Acutely Exposed to High Altitude. Prehospital Emerg Care. 2022;0(0):1-8. doi:10.1080/10903127.2022.2126912
39. Johnson D, Bates S, Nukalo S, Staub A, Hines A, Leishman T, Michel J, Sikes D, Gegel B, Burgert J. The effects of QuikClot combat gauze on hemorrhage control in the presence of hemodilution and hypothermia. Ann Med Surg (Lond). 2014 Mar 26;3(2):21-5.
40. Sauer A, Dierks A, Wolfschmidt F, Hassold N, Bley TA, Kickuth R. Hemostatic wound dressing for postinterventional hemostasis in large femoral artery access sites: an initial efficacy and safety Study. Journal of Endovascular Therapy. 2016;23(5):744-750.
41. Mobaraki, M., Karnik, S., Li, Y., & Mills, D. K. (2022). Therapeutic Applications of Halloysite. Applied Sciences, 12(1), 87. https://doi.org/10.3390/app12010087
42. Alavi, M.; Totonchi, A.; Okhovat, M.A.; Motazedian, M.; Rezaei, P.; Atefi, M. The effect of a new impregnated gauze containing bentonite and halloysite minerals on blood coagulation and wound healing. Blood Coagul. Fibrinolysis, 2014: 25, 856–859.
43. Masoud, A.-R.; Alakija, F.; Perves Bappy, M.J.; Mills, P.A.S.; Mills, D.K. Metallizing the surface of halloysite nanotubes—a review. Coatings 2023, 13, 542. https:// doi.org/10.3390/coatings13030542
44. Yan, D., Li, Y., Liu, Y., Li, N., Zhang, X., & Yan, C. Antimicrobial properties of chitosan and chitosan derivatives in the treatment of enteric infections. Molecules, 2021: 26(23), 7136. https://doi.org/10.3390/molecules26237136
45. Zhao, P., Feng, Y., Zhou, Y., Tan, C., & Liu, M. Gold@Halloysite nanotubes-chitin composite hydrogel with antibacterial and hemostatic activity for wound healing. Bioactive Materials, 2023; 20, 355-367. https://doi.org/10.1016/j.bioactmat.2022.05.035
46. Li, S., Jiang, M., Zhang, Y., Xie, X., Li, W., Ming, P., Jiang, X., Yang, B., He, Y., Chen, J., & Tao, G. Multi-functional carboxymethyl chitosan/sericin protein/halloysite composite sponge with efficient antibacterial and hemostatic properties for accelerating wound healing. International Journal of Biological Macromolecules, 2023; 234, 123357. https://doi.org/10.1016/j.ijbiomac.2023.123357
47. Chen, J., Mo, Y., Zhang, X., Zhang, S., Cui, A., Wang, X., & Li, J. Solution-blow spinning halloysite nanotube loaded chitosan-polyethylene oxide fibrous membrane as hemostatic dressings. Applied Clay Science, 2024; 262, 107597. https://doi.org/10.1016/j.clay.2024.107597